Membrane cholesterol modulates dihydropyridine receptor function in mice fetal skeletal muscle cells

Sandrine Pouvreau[1], Christine Berthier[1], Sylvie Blaineau[1], Jacqueline Amsellem[1], Roberto Coronado[2] and Caroline Strube[1]

[1] *Laboratoire de Physiologie des Eléments Excitables, UMR CNRS 5123, UCB-Lyon 1, 69622 Villeurbanne Cedex, France*
[2] *Department of Physiology, University of Wisconsin, Madison, WI 53706, USA*

Caveolae and transverse (T-) tubules are membrane structures enriched in cholesterol and glycosphingolipids. They play an important role in receptor signalling and myogenesis. The T-system is also highly enriched in dihydropyridine receptors (DHPRs), which control excitation–contraction (E–C) coupling. Recent results have shown that a depletion of membrane cholesterol alters caveolae and T-tubules, yet detailed functional studies of DHPR expression are lacking. Here we studied electrophysiological and morphological effects of methyl-β-cyclodextrin (MβCD), a cholesterol-sequestering drug, on freshly isolated fetal skeletal muscle cells. Exposure of fetal myofibres to 1–3 mm MβCD for 1 h at 37°C led to a significant reduction in caveolae and T-tubule areas and to a decrease in cell membrane electrical capacitance. In whole-cell voltage-clamp experiments, the L-type Ca^{2+} current amplitude was significantly reduced, and its voltage dependence was shifted ∼15 mV towards more positive potentials. Activation and inactivation kinetics were slower in treated cells than in control cells and stimulation by a saturating concentration of Bay K 8644 was enhanced. In addition, intramembrane charge movement and Ca^{2+} transients evoked by a depolarization were reduced without a shift of the midpoint, indicating a weakening of E–C coupling. In contrast, T-type Ca^{2+} current was not affected by MβCD treatment. Most of the L-type Ca^{2+} conductance reduction and E–C coupling weakening could be explained by a decrease of the number of DHPRs due to the disruption of caveolae and T-tubules. However, the effects on L-type channel gating kinetics suggest that membrane cholesterol content modulates DHPR function. Moreover, the significant shift of the voltage dependence of L-type current without any change in the voltage dependence of charge movement and Ca^{2+} transients suggests that cholesterol differentially regulates the two functions of the DHPR.

(Received 17 September 2003; accepted after revision 5 January 2004; first published online 14 January 2004)
Corresponding author C. Strube: *LNPC, CNRS UMR 6150*, Faculté Médecine Nord, Bd Pierre Dramard, 13916 Marseille Cedex 20, France. Email: strube.c@jean-roche.univ-mrs.fr

Ca^{2+} flux across the cell membrane into the myoplasm is required during several stages of muscle development including myoblast fusion (Seigneurin-Venin *et al.* 1996; Bijlenga *et al.* 2000) and late-stage differentiation into multinucleated myotubes (Shainberg *et al.* 1969; Morris & Cole, 1979; Salzberg *et al.* 1995). The cellular mechanisms and sites of regulation of Ca^{2+} influx in developing muscle cells are poorly understood. In striated muscle cells, the highest density of voltage-dependent dihydropyridine receptor (DHPR) L-type Ca^{2+} channels is found in the transverse tubular system (Siri *et al.* 1980; Potreau & Raymond, 1980; Almers *et al.* 1981; Jorgensen *et al.* 1989; Romey *et al.* 1989), where these channels control excitation–contraction (E–C) coupling (Rios & Brum, 1987). DHPRs are also found in discrete foci in the sarcolemmal region of the myofibres corresponding to caveolae (Jorgensen *et al.* 1989). Other Ca^{2+} channel types, such as T-type Ca^{2+} channels have been described in developing skeletal muscle (Beam & Knudson, 1988; Berthier *et al.* 2002). They are preferentially located at the surface membrane (Romey *et al.* 1989) and could be involved in the early stages of muscle differentiation (Bijlenga *et al.* 2000; Berthier *et al.* 2002). Moreover, peripheral couplings established between the plasma membrane and the sarcoplasmic reticulum play a significant functional role in fetal myotubes (Takekura *et al.* 1994). Hence, control of Ca^{2+} influx in muscle cells could involve different types of Ca^{2+} channels at different

 DOI: 10.1113/jphysiol.2003.055285

locations. Recent work suggests that plasma membrane caveolae regulate intracellular Ca^{2+} influx and receptor-mediated signal transduction pathways in many cell types (for review see Isshiki & Anderson, 1999). Since caveolae and the nascent T-system may have a common anatomical origin (Yuan *et al.* 1990, 1991; Flucher *et al.* 1991), these two locations could play a role in the control of Ca^{2+} influx at different stages of muscle cell development.

Caveolae are 50–100 nm 'omega-shaped' specialized microdomains of the plasma membrane. These membrane invaginations of the cell surface are characterized by a light buoyant density, a resistance to solubilization by Triton X-100 at 4°C and enrichment in glycosphingolipids, cholesterol, sphingomyelin, and lipid anchored membrane proteins (Shaul & Anderson, 1998). Caveolae are also enriched in a 21–24 kDa characteristic membrane protein, called caveolin. The expression of caveolin-3, which is limited to muscle cells of all types (skeletal, cardiac and smooth muscle cells), is regulated during muscle development (Biederer *et al.* 2000) and is associated with both caveolae and T-tubules system in developing and mature skeletal muscle fibres (Parton *et al.* 1997; Ralston & Ploug, 1999). These results, combined with early morphological studies, suggest that caveolae and caveolin-3 may be involved in the development of transverse tubules during myogenesis (Ishikawa, 1968; Franzini-Armstrong, 1991).

The T-tubule membrane system of striated muscle cells, like caveolae, is highly enriched in cholesterol (Rosemblatt *et al.* 1981). Several studies have demonstrated that the cholesterol content of plasma membrane influences intracellular Ca^{2+} homeostasis and transmembrane Ca^{2+} flux (for review see Bastiaanse *et al.* 1997). In smooth and cardiac muscle cells (Gleason *et al.* 1991; Sen *et al.* 1992; Bastiaanse *et al.* 1994), cholesterol enrichment of the plasma membrane was associated with an increase in intracellular Ca^{2+} and in Ca^{2+} flux through L-type Ca^{2+} channels. In contrast, cholesterol depletion caused a decrease in frequency, amplitude and the spatial dimension of Ca^{2+} sparks in arterial smooth muscle cells and neonatal cardiomyocytes (Löhn *et al.* 2000), and a decrease in depolarization-induced muscle tension in skinned skeletal muscle fibres (Launikonis & Stephenson, 2001). Although the mechanisms by which plasma membrane cholesterol enrichment or depletion affect Ca^{2+} homeostasis are not clear, the structural and functional integrity of the T-system and caveolae are known to depend on the presence of membrane cholesterol. In epithelial cell lines, exposure to cholesterol-binding agents flattened the shape of caveolae (Rothberg *et al.* 1990; Chang *et al.* 1992) and in skeletal muscle, cholesterol binding drugs caused a redistribution of T-tubule protein markers and a dramatic reduction in the extent of surface-connected tubular elements (Carozzi *et al.* 2000). Furthermore, absolute cellular levels of cholesterol need to rise above a certain threshold before caveolae formation can occur (Hailstones *et al.* 1998). Hence, one of the consequences of cholesterol enrichment or depletion may be to modify the density and functional state of caveolae and T-tubules where muscle Ca^{2+} homeostasis might be critically regulated.

The aim of this study was to examine the effect of membrane cholesterol depletion on skeletal muscle Ca^{2+} channels and E–C coupling. In this work, freshly isolated skeletal muscle myofibres from mice fetuses were treated with methyl-β-cyclodextrin (MβCD), which removes cell membrane cholesterol from viable cells (Kilsdonk *et al.* 1995; Yancey *et al.* 1996; Christian *et al.* 1997; Gimpl *et al.* 1997; Steck *et al.* 2002). We investigated the effect of MβCD treatment on Ca^{2+} currents, charge movements, voltage-evoked Ca^{2+} transients and membrane ultrastructure. We show that in our preparation MβCD produced morphological changes in the nascent T-tubule membrane network. Additionally, MβCD treatment modified L-type Ca^{2+} current properties and weakened E–C coupling. Altogether, our results indicate that membrane cholesterol modulates DHPR function by several mechanisms. Part of this work has been published in abstract form (Strube *et al.* 2002; Pouvreau *et al.* 2003).

Methods

Single cell preparation

All experiments, except for those examining T-tubule ultrastructure (see below), were performed on freshly isolated intercostal myotubes from 18-day-old mouse fetuses (Swiss OF1 from IFFA CREDO, l'Arbresle, France). Pregnant mice and fetuses were killed by cervical dislocation and decapitation, respectively, in accordance with ethical guidelines laid down by the French directives for care of laboratory animals (decree 87–848). The two half-ribcages of each fetus were dissected in Krebs solution containing (mM): 140 NaCl, 5 KCl, 2.5 $CaCl_2$, 1 $MgCl_2$, 10 Hepes-NaOH, pH 7.4. The tissues were incubated at 37°C for about 12 min in phosphate-buffered saline (Sigma, St Quentin Fallavier, France), containing 3 mg ml^{-1} collagenase (type I, Sigma) and 1 mg ml^{-1} trypsin (type III, Sigma). Cells were then mechanically dispersed and collected in plastic Petri dishes (35 mm diameter) containing Krebs solution for the control conditions. The treated cells were incubated at 37°C for 1 h in Krebs containing either methyl-β-cyclodextrin (MβCD, Sigma)

or a mixture of cholesterol and MβCD (cholesterol–water soluble, Sigma). Concentrations of 1–5 mM MβCD were used and had a similar effect. For the cholesterol-treated cells, the molar ratio cholesterol/MβCD was 1/5 and the final concentration of MβCD was 1.4 mM. As a control, we also checked that the incubation at 37°C by itself did not affect cell properties.

Electrophysiological measurements

The standard patch-clamp technique was used in the whole-cell recording configuration. Recordings were made with an Axopatch 200B patch-clamp amplifier (Axon Instruments, Foster City, CA, USA) at room temperature. Leak currents and linear capacity (for charge movement recordings) were compensated with the amplifier's circuit. Series resistance, R_s, was analogically compensated close to the point of amplifier oscillation with the amplifier's circuit. The voltage drop due to series resistance ($R_s \times I_{max}$) was checked for each cell and never exceeded 6 mV. The average value was 2.66 ± 0.14 mV ($n = 102$). The average time lag needed to charge the membrane capacitance ($R_s \times C_m$) was 0.40 ± 0.01 ms ($n = 102$) and never exceeded 0.70 ms. Data acquisition and command voltage pulse generation were performed with a Digidata 1200 interface controlled by pCLAMP software (Axon Instruments). Data were filtered at 1 kHz and digitized at 2–10 kHz. Cell capacitance was determined by integration of a capacity transient elicited by a 10 mV hyperpolarizing pulse from a holding potential of −80 mV. Ca^{2+} currents were measured from a holding potential of −80 mV. Test pulses of 500 ms in 10 mV increments to potentials ranging from −70 to +60 mV were applied. A 750 ms prepulse to −30 mV was used to inactivate T-type Ca^{2+} currents and to isolate L-type Ca^{2+} currents. The charge movement protocol consisted of a 25 ms test pulse P (in 10 mV increments ranging between −50 and +60 mV) from a holding potential of −80 mV. Subtraction of the linear component was assisted by a $P/4$ procedure preceding the test pulse. $P/4$ hyperpolarizing prepulses were separated by 500 ms and had a duration of 25 ms. An alternative protocol that eliminated immobilization-sensitive components in myotubes in culture (Adams *et al.* 1990; Strube *et al.* 1996) was also used and gave qualitatively similar results.

Ca^{2+} transient measurements

Ca^{2+} transients were measured using a confocal microscope in line-scan mode as previously described (Ahern *et al.* 2001). Cells were loaded with 5 μM fluo-4 (fluo-4 acetoxymethyl (AM) ester, Molecular Probes, Eugene, OR, USA) for 1 h at room temperature. Stocks of fluo-4 (1 mg ml^{-1}) were made in DMSO and stored frozen. All experiments were performed at room temperature. Cells were viewed with an inverted Olympus microscope with a × 20 objective and a Fluoview confocal attachment (Olympus, Melville, NY, USA). The 488 nm spectrum line necessary for fluo-4 excitation was provided by a 5 mW argon laser attenuated to 6–20% with neutral density filters. The pinhole aperture was 100–150 μm. Excitation was separated from emission with a dicroic mirror DM 488/543 followed by a long pass filter at 510 nm. The dimensions of the line-scan images were 512 pixels per line with a pixel size of 0.25 μm and 1000 lines per image. The z-axis resolution was ∼0.8 μm. The line-scan rate was 2.05 ms per 512-pixel line. The fluorescence intensity, F, was calculated by densitometric scanning of line-scan images and was averaged over the entire width of the cell. The background fluorescence intensity (F_0) was averaged in the same manner from areas of the same image prior to the voltage pulse. The fluorescence unit F corresponds to $(F - F_0)/F_0$. A compressed 32-colour table and an 8-pixel running average (smoothing) were applied to all images to highlight the Ca^{2+} transient. The pixel intensity as a function of time and space was obtained directly from the line-scan image with tools provided by National Institutes of Health-Image 1.6 (National Institutes of Health, Bethesda, MD, USA). A complete patch-clamp set-up was coupled to the confocal microscope to control the membrane potential. Ca^{2+} transients were evoked every 30 s in response to 50 ms depolarizing pulses in −20 mV increments to potentials ranging from +60 to −40 mV from a holding potential of −80 mV.

Solutions

Action potentials were recorded in Krebs solution containing (mM): 140 NaCl, 5 KCl, 2.5 $CaCl_2$, 1 $MgCl_2$, 10 Hepes-NaOH, pH 7.4, and the pipette solution contained (mM): 140 KCl, 1 $MgCl_2$, 0.5 EGTA, 10 MOPS-KOH, pH 7.2. The external solution for Ca^{2+} current recordings and Ca^{2+} transient measurements contained (mM): 130 TEA methanesulphonate, 10 $CaCl_2$, 1 $MgCl_2$, 10^{-3} TTX, 10 Hepes-TEA(OH), pH 7.4. The pipette solution consisted of (mM): 140 caesium aspartate, 5 $MgCl_2$, 5 EGTA (Ca^{2+} currents) or 0.1 EGTA (Ca^{2+} transients), 10 Mops-CsOH, pH 7.2. For charge movement recordings 0.5 mM Cd^{2+} and 0.2 mM La^{3+} were added to the external solution and caesium was replaced by N-methyl glucamine in the internal solution.

Data analysis

Data analysis and curve fitting were done using pCLAMP (Axon Instruments) and Sigmaplot (Jandel, San Rafael, CA, USA). Statistical tests were performed with Instat (GraphPad Software Inc, San Diego, CA, USA).

The voltage dependence of the L-type Ca^{2+} current curves was fitted with a smooth curve according to eqn (1):

$$I_L(V) = G_{max}(V - V_{rev})/\{1 + \exp[(V_{1/2,G} - V)/k_G]\} \quad (1)$$

where $I_L(V)$ is the peak current in response to the test depolarizing potential V, V_{rev} is the apparent reversal potential (determined as one of the fitted parameters), G_{max} is the maximum conductance for the peak current, $V_{1/2,G}$ is the potential that elicits the half-maximum increase in conductance, and k_G is a steepness parameter. This fit allowed us to determine I_{max}, the peak of this fit, and the corresponding potential, V_{Imax}. Ca^{2+} conductance *versus* voltage curves were calculated from eqn (2) using the V_{rev} value obtained from the fit of the $I_L(V)$ curve with eqn (1):

$$G(V) = I(V)/(V - V_{rev}) \quad (2)$$

As previously described (Strube *et al.* 2000), the time course of the macroscopic L-type Ca^{2+} current was fitted by the sum of two exponential components according to eqn (3):

$$I(t) = A_1\exp(-t/\tau_1) + A_2\exp(-t/\tau_2) + C \quad (3)$$

where $I(t)$ is the current density at time t after the onset of the depolarization, τ_1 and τ_2 are the time constants for the two components of the current time course, C is the steady-state current, and A_1 and A_2 are the amplitudes for each component.

For each cell, or for the population average, the voltage dependence of Ca^{2+} conductance (G), charge movements (Q), and fluorescence variation (F) were fitted according to a Boltzmann equation (eqn (4)):

$$A(V) = A_{max}/\{1 + \exp[-(V - V_{1/2,A})/k]\} \quad (4)$$

where A_{max} was either G_{max}, Q_{max} or F_{max}; $V_{1/2,A}$ is the potential at which $A = A_{max}/2$; and k is the slope factor.

In all figures, the symbols and error bars correspond to the population mean ± S.E.M. of n experiments. The curves correspond to a fit to the mean values. The statistical differences between control and MβCD-treated groups were made using the non-parametric Mann-Whitney test. The significance level was set at $P < 0.05$.

Di-8-ANEPPS image analysis

MβCD-treated or untreated freshly isolated myotubes were stained in Krebs solution containing 8.5 mM Di-8-ANEPPS (Molecular Probes) for up to 10 min followed by dye washout. Cells were then viewed with the same inverted microscope, filters and confocal attachment as for Ca^{2+} measurements, except that we used a 40 × oil-immersion objective (NA = 1.3). 2D images (1024 × 1024 pixels) of Di-8-ANEPPS fluorescent labelling were Kalman-averaged three times and analysed with Scion Image software (PC version of NIH Image developed by Scion corporation, MD, USA). The 2D orientation of labelled T-tubule membrane structures was analysed for each image using a standard method, as follows. Images were first rotated to identically orientate all myofibres: the major axis of each cell was arbitrarily set so that it made a 45 deg angle with the x-axis of the image. A region of interest, comprising the entire surface of the optical section of the labelled cell excluding the surface membrane, was then defined manually. The grey level distribution of each thus-defined region of interest was arithmetically standardized, setting the maximum grey level value at 255 and the mean grey level value at 127. The threshold was arbitrarily set to eliminate pixels with a grey level value inferior to 130–135, resulting in background-labelling elimination. Images were then binarized and noise-reduced by erosion. The orientation of stained profiles larger than 20 pixels, i.e. the angle made by the main axis of each profile with the x-axis of the image, was then automatically determined. These angles, measured on six MβCD-treated cells and seven control cells, were pooled and plotted on a histogram that thus displayed the distribution of the orientation of T-tubule profiles for each cell category.

Ultrastructural study

For observation of caveolae, MβCD-treated or untreated freshly isolated fetal intercostal muscles were fixed at room temperature for 60 min with 2% glutaraldehyde, then postfixed for 30 min with 1% osmium tetroxide, and finally dehydrated and embedded. Sections were stained with uranyle acetate and lead citrate and examined with a Philips CM 120 electron microscope. For T-tubule observation, the two half-ribcages of an 18-day-old mouse fetus were dissected in Krebs solution. One half-ribcage was incubated at 37°C for 1 h in Krebs containing 6 mM MβCD, the other one was incubated under the same conditions in normal Krebs. The electrophysiological effect of MβCD under these experimental conditions was controlled in preliminary experiments on myotubes

dissociated after MβCD incubation and was found to be the same as on fibres treated with MβCD after dissociation. After the incubation, each half-ribcage was rinsed and fixed in 2% glutaraldehyde–1.6% paraformaldehyde in 100 mM cacodylate buffer, pH 7.3 for 150 min. Specimens were washed five times in buffer and rinsed overnight at 4°C in 150 mM cacodylate buffer. Small pieces of intercostal muscle were post-fixed for 150 min with vibratory agitation at room temperature in 1% osmium tetroxide–2% lanthanum nitrate in a 100 mM S-collidine buffer at pH 7.4. Specimens were then rapidly dehydrated, and embedded in epon. Tissue sections were examined using a Jeol 1200 EX electron microscope.

Digital images taken for caveolae and T-tubule observations were analysed with AnalySIS (Soft Imaging System, Eloïse, Roissy, France). For observation of caveolae, we first measured the length of linear sarcolemma without including the invaginations of the surface membrane and then measured the perimeter of each caveolae and totted up these perimeters. The ratio of caveolae length to sarcolemma length was used as an estimation of the caveolae density. For observation of T-tubules, the length of T-tubule labelled profiles and the surface of the fibres (except the nucleus area) were measured on fibres orientated parallel to the section plan. The ratio of the two values was used as an estimation of T-tubule density.

Chemicals

Deionized glass-distilled water was used in all solutions. All salts were reagent grade. Bay K 8644 (Calbiochem, La Jolla, CA, USA) was made as a 5 mM stock solution in absolute ethanol and stored in light-resistant containers.

Results

To determine gross anatomical changes in the nascent T-tubule system produced by MβCD, cells were incubated with Di-8-ANEPPS. Di-8-ANEPPS is a membrane-impermeant fluorescent dye that intercalates in the outer leaflet of the cell surface membrane and of the surface-connected membranes such as the T-system (Shacklock *et al.* 1995). Figure 1*A* shows a confocal image in reverse colour (black represents high-intensity fluorescence) of a freshly isolated intercostal muscle cell from an 18-day-old

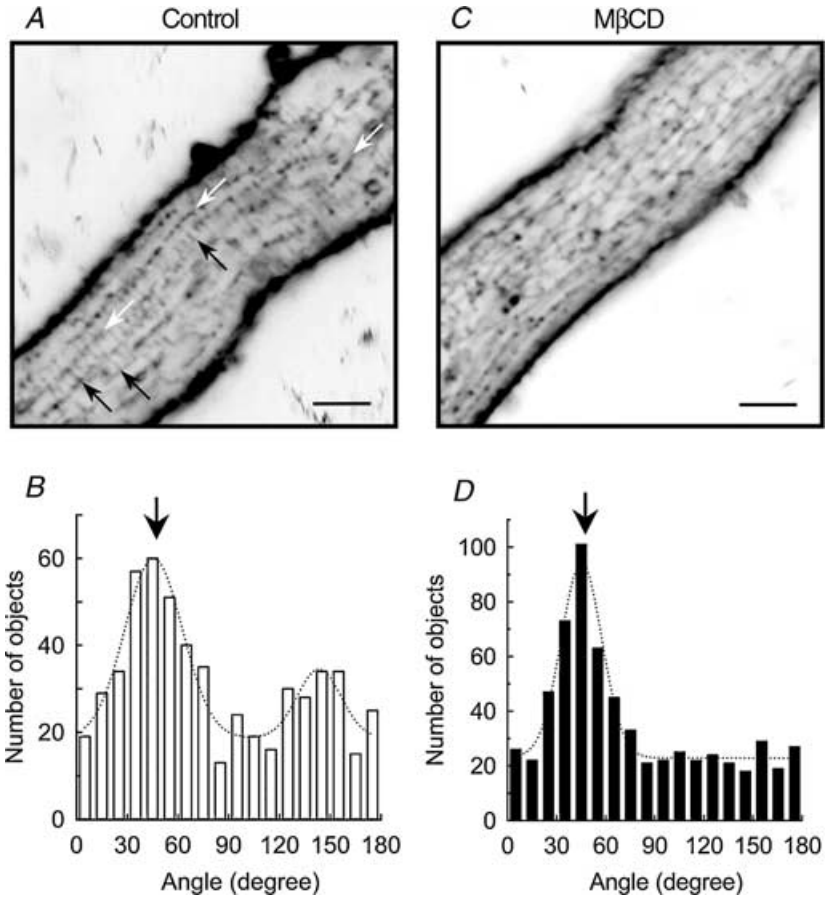

Figure 1. The T-tubule system is disorganized in MβCD-treated muscle fibres
A and *C*, freshly isolated intercostal muscle cells from 18-day-old fetuses stained with Di-8-Anepps in control conditions (*A*) and after MβCD treatment (*C*). White arrows indicate 'beaded' stained lines running parallel to the cell surface, black arrows indicate weakly stained line orientated perpendicular to the cell surface. Scale bars = 5 μm. *B* and *D*, computed histogram of the orientation of all identified objects of the binary image (see Methods) obtained by analysing 7 control cells (*B*) or 6 MβCD-treated cells (*D*). The dotted line is a fit to the data using one or two Gaussian curves. The arrow indicates the angle that the main axis of the cell made with a vertical axis, i.e. 45 deg.

fetus incubated with 8.5 mM Di-8-ANEPPS for 10 min at room temperature. The staining pattern was inspected at different focal planes and the most salient features which are shown by the arrows consisted of strings of dots or 'beaded' lines running parallel to the cell surface (white arrows) and of weakly stained fine line-like elements with a direction perpendicular to the cell surface (black arrows). The orientation of the beaded lines is consistent with the longitudinal orientation of the T-system seen at early stages of development (Franzini-Armstrong, 1991; Takekura *et al.* 2001) and the orthogonal line-like elements could represent connections between the longitudinal elements. To quantify the orientation of all objects in the image, we measured the angle that each object made with a vertical line after binarizing and eroding the image (Methods). A histogram of the orientation of all identified objects in the binary image with respect to the vertical axis is shown in Fig. 1*B* for seven cells. The main orientation of the cell is indicated by the arrow and represents a 45 deg angle with the vertical. The histogram shows that most of the objects in the cell were orientated either parallel to the long axis of the cell (45 deg angle) or perpendicular to the cell length (135 deg angle). Figure 1*C* shows a confocal image of a muscle cell treated with 3 mM MβCD for 1 h at 37°C prior to the Di-8-ANEPPS staining, and data from six similar fibres are computed in the histogram in Fig. 1*D*. In MβCD-treated cells the majority of the objects are orientated longitudinally (parallel to the long axis of the cell) whereas objects with a transverse orientation (perpendicular to the cell) were not stained by Di-8-ANEPPS. This result suggested that MβCD treatment produced a drastic

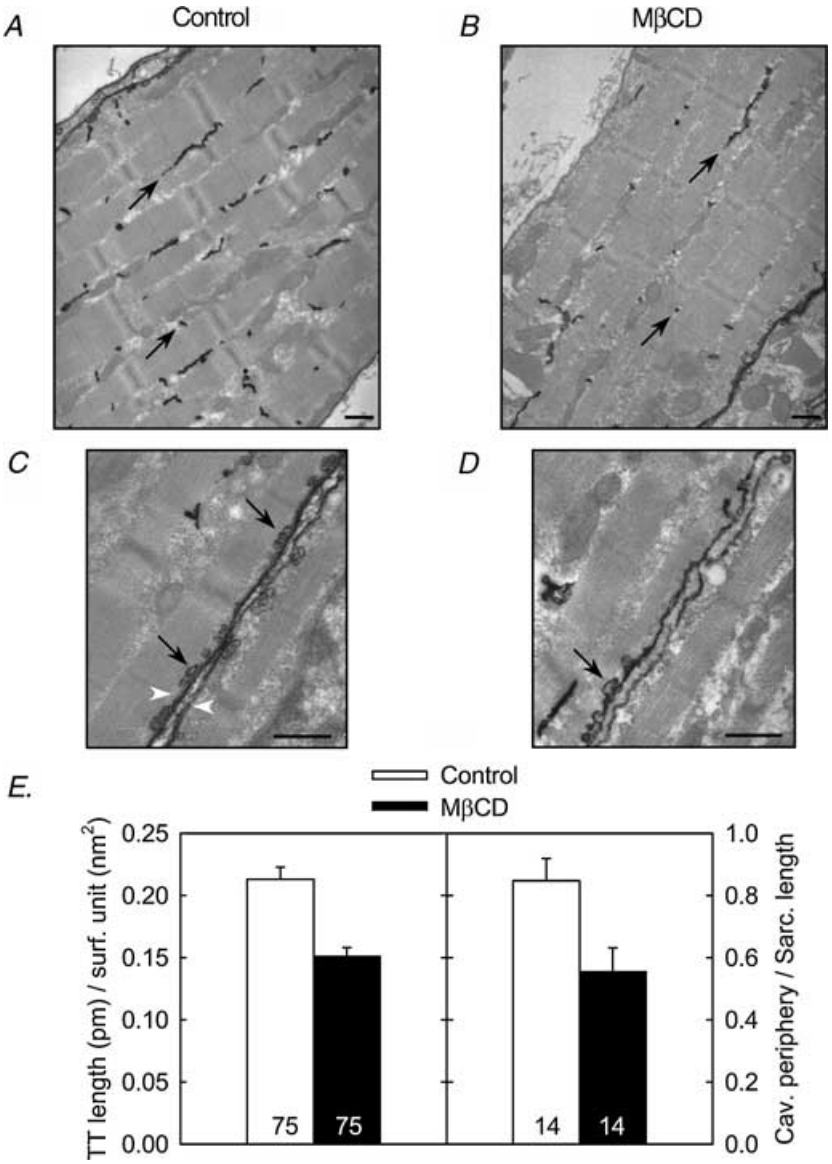

Figure 2. MβCD treatment reduces the amount of caveolae and T-tubules connected to the membrane
A–D, electron microscopy pictures of control (*A*, *C*) and MβCD-treated (*B*, *D*) 18-day-old fetus intercostal muscles stained with lanthanum. Black arrows indicate lanthanum-labelled T-tubules (*A*, *B*) and lanthanum-labelled caveolae (*C*, *D*). White arrowheads indicate sarcolemma of two apposite cells. Scale bars = 500 nm. *B*, histogram of the amount of T-tubules (right) and caveolae (left) connected to the membrane before and after MβCD treatment. The number indicated at the bottom of each bar corresponds to the number of measurements included in the corresponding bar. Values for MβCD-treated cells are significantly different ($P < 0.02$, Mann-Whitney test) from the control values.

Table 1. Parameter values of action potentials recordings

	n	Amplitude (mV)	Half-width (ms)	Max. rate of rise (mV ms^{-1})	Max. rate of decay (mV ms^{-1})
Control	5	113.3 ± 10.2	2.61 ± 0.41	132.2 ± 20.2	−53.7 ± 8.8
MβCD	6	106.9 ± 3.4	2.81 ± 0.20	124.2 ± 15.4	−42.0 ± 3.3

Action potentials recorded in current clamp were evoked from a holding potential of −80 mV by 10 ms pulses. None of the values obtained in treated-cells are significantly different from the corresponding control values (Mann-Whitney test).

Table 2. Parameter values of the I_L–V curve fits

	n	C (pF)	G_{max} (nS)	$V_{1/2,G}$ (mV)	k_G (mV)	V_{rev} (mV)	I_{max} (nA)
Control	32	296.5 ± 19.2	58.8 ± 4.5	12.7 ± 1.2	5.2 ± 0.2	71.4 ± 2.0	−2.47 ± 0.18
MβCD	20	224.4 ± 20.3*	34.5 ± 2.9**	29.0 ± 1.7**	6.7 ± 0.3**	73.8 ± 1.9	−0.89 ± 0.15**
MβCD + cholesterol	9	306.4 ± 35.9	54.4 ± 4.4	15.9 ± 2.1	6.1 ± 0.3*	74.2 ± 3.5	−2.26 ± 0.27

All the parameters were calculated as described in Methods. C is the membrane capacitance of the cell, G_{max} is the maximum conductance for the peak current, $V_{1/2,G}$ is the potential that elicits the half-maximum increase in conductance, k_G is a steepness factor, I_{max}, is the peak of the I_L–V curve fit and V_{rev} the corresponding potential. Data are given as mean ± S.E.M. and were obtained by fitting the data from *n* fibres in each group. Asterisks indicate values which are significantly different (*$P < 0.05$; **$P < 0.001$) from the corresponding control values (Mann-Whitney test).

disorganization of the nascent T-tubule system and an overall loss of spatial complexity in this membrane network.

To further explore the effect of the MβCD on membrane ultrastrucuture, we performed electron microscopy on muscles stained with lanthanum, which is an electron-dense extracellular tracer that outlines caveolae and the T-tubule system (Minetti *et al.* 2002). Representative images from a control and from a MβCD-treated cell are shown in Fig. 2*A*–*D*. Two sets of measurements were done on two different populations of cells as described in Methods. First, we measured the total length of the T-tubules stained with lanthanum and divided this number by the corresponding cell surface on 75 images taken from 38 control (untreated) cells (Fig. 2*A*) and 75 images taken from 38 MβCD-treated cells (Fig. 2*B*). The average ratio values obtained are summarized in the left histogram of Fig. 2*E* which shows that the density of lanthanum-labelled T-tubules was reduced in MβCD-treated fibres. On a different group of myotubes (14 images from 4 control fibres, Fig. 2*C*, and 14 images from 4 MβCD-treated fibres, Fig. 2*D*), we measured the total caveolae perimeter and the corresponding linear sarcolemma length. The results are summarized in the right histogram of Fig. 2*E*, which shows that the number of caveolae is reduced in MβCD-treated fibres compared to control cells. Altogether, these morphological studies are consistent with the confocal images. They suggest that a significant proportion of the membrane invaginations were disconnected from the surface membrane in MβCD-treated cells.

Global changes in cell surface and surface-connected areas after MβCD treatment were estimated by electrical capacitance measurements in voltage-clamped cells. In these experiments, 21 control and 36 MβCD-treated fibres were imaged under phase contrast at 320 × magnification to obtain the visual surface. The two-dimensional cell area or visual surface was measured with Lucia Analysis software (Nikon, Champigny sur Marne, France). Cell membrane capacitance was then measured in the same cell after establishing the whole-cell configuration. Figure 3 shows the membrane capacitance plotted as a function of the visual surface for the same cell. The continuous lines correspond to a linear fit to the values of each population of cells. The graph shows that for an equal visual surface (mean values of 10773 ± 510 and 10106 ± 533 μm^2 for control and treated cells, respectively), membrane capacitance was significantly reduced in MβCD-treated cells (279.9 ± 17.7 and 206.4 ± 12.2 pF for control and treated cells, respectively, $P < 0.002$ Mann-Whitney test). Since membrane capacitance was significantly different between control and MβCD-treated cells, the electrophysiological data below have not been normalized with respect to the cell capacitance. Instead, control and MβCD-treated cells were selected by eye on the basis of a comparable visual surface.

To check the excitability of the fibres, action potentials evoked by 10 ms pulses from a holding potential of

−80 mV in control and MβCD-treated cells were recorded under current clamp. Four parameters were measured to allow a comparison between the two populations of fibres: the amplitude of the action potential, its duration at its half-maximum amplitude, the maximum rate of rise and the maximum rate of decay (Table 1). None of these parameters recorded in treated cells was significantly different from the corresponding value in control cells, suggesting that the excitability of the fibres was not drastically affected by MβCD treatment.

Ca^{2+} currents in control and MβCD-treated cells were recorded with whole-cell voltage clamp in external and pipette solutions designed to isolate Ca^{2+} current from other currents in the cell. Figure 4*A* shows representative whole-cell Ca^{2+} current recordings obtained in control and MβCD-treated cells in response to 500 ms depolarizing voltage steps from a holding potential of −80 mV. From this holding potential, we observed both T-type and L-type Ca^{2+} currents, in agreement with previous results (Beam & Knudson, 1988; Shimahara & Bournaud, 1991; Strube *et al.* 2000; Berthier *et al.* 2002). Currents are shown for step depolarizations to −20 and +30 mV where either T- or L-type currents are dominant, respectively. The records clearly show that L-type Ca^{2+} current was reduced in MβCD-treated myotubes. The average I_{Ca}–V curves shown in Fig. 4*B* confirmed this result. Whereas T-type Ca^{2+} current was not affected by the MβCD treatment, the maximum amplitude of L-type current was reduced ∼3-fold and its voltage dependence was shifted ∼15 mV towards more positive potentials.

In order to test if MβCD could modify the L-type Ca^{2+} channel by a mechanism other than cholesterol removal, we recorded L-type Ca^{2+} current from myotubes incubated in the presence of 1.4 mM MβCD saturated with cholesterol (molar cholesterol/MβCD ratio = 1/5). Since MβCD acts as a cholesterol carrier, this procedure is usually used as a control to demonstrate that the cholesterol-saturated MβCD is unable to affect membrane processes (Launikonis & Stephenson, 2001) in the same way as MβCD by itself. To isolate L-type Ca^{2+} currents, a 750 ms prepulse to −30 mV was used to inactivate T-type Ca^{2+} currents. I_L–V curves from control, MβCD-treated or MβCD + cholesterol-treated cells are shown in Fig. 5*A*. Whereas MβCD alone reduced L-type Ca^{2+} current amplitude by ∼65% and shifted the voltage dependence, MβCD + cholesterol did not significantly affect the L-type Ca^{2+} current (Fig. 5 and Table 2). From this result, we may conclude that the effect of MβCD was due to membrane cholesterol removal rather than to a direct pharmacological effect on the DHPR.

In the following experiments we further investigated the effect of MβCD treatment on the gating and kinetic

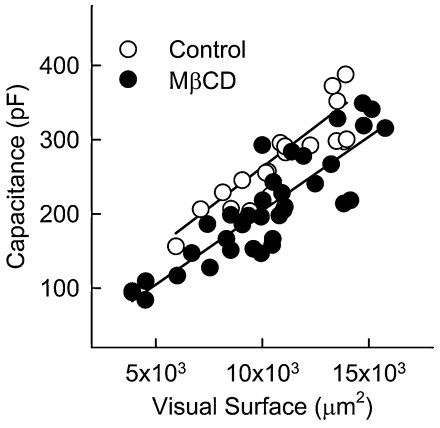

Figure 3. For a constant visual surface, cell membrane capacitance is reduced in MβCD-treated cells
Cell membrane capacitance is plotted as a function of the visual surface for 21 control cells and 36 MβCD-treated cells. The continuous lines correspond to a linear fit to the values of each population of cells.

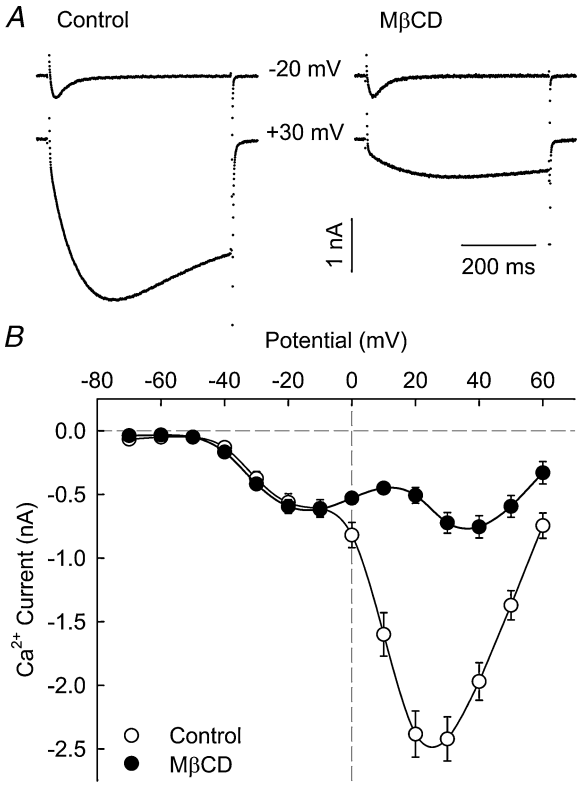

Figure 4. MβCD treatment decreases L-type Ca^{2+} current amplitude without significantly affecting T-type Ca^{2+} current
A, representative Ca^{2+} current recordings in response to 500 ms depolarizing pulses from a holding potential of −80 mV to the indicated potential in control and MβCD-treated fibres. *B*, averaged voltage dependence of Ca^{2+} current obtained from 38 control and 40 MβCD-treated cells.

properties of L-type Ca^{2+} channels. After the 750 ms prepulse to −30 mV used to inactivate T-type Ca^{2+} current, test pulses of 500 ms (for *I–V* curves) or 1500 ms (for kinetic analysis) were applied between −30 and +60 mV in 10 mV increments. Figure 5*B* shows Ca^{2+} conductance *versus* voltage curves computed as described in Methods with eqns (1) and (2). The continuous lines correspond to a Boltzmann fit to the population mean while mean parameters fitted to each cell are shown in Table 2. These data show that the maximum conductance, G_{max}, was significantly reduced (∼40%) in MβCD-treated cells, but not significantly affected in MβCD + cholesterol-treated cells. Moreover, scaling the fit of the MβCD-treated population (dotted line) to that of control cells indicated clearly that the half-activation potential, $V_{1/2,Q}$, was shifted 16 mV towards positive potentials. However, the apparent reversal potential, V_{rev}, was not significantly different (see Table 2). Figure 6 summarizes the results of a kinetic analysis of L-type Ca^{2+} current. We noticed that MβCD treatment increased the time to peak ∼1.5-fold (results not shown). The fit of the macroscopic L-type current as a sum of two exponential components (see Methods) allowed us to evaluate changes in activation and inactivation kinetics. As shown in Fig. 6*A*, in most cases the time course of the current in response to a test potential larger than 0 or 10 mV for control or MβCD-treated cells, respectively, was well described by eqn (3). For smaller depolarizations the current was too slow and displayed little if any inactivation. Figure 6*B* illustrates activation and inactivation time constants *versus* potential. Both the activation and inactivation time constants were significantly larger at all test potentials, indicating that MβCD slowed the Ca^{2+} current kinetics. Altogether, these results show that cholesterol removal modified gating properties of L-type Ca^{2+} channels.

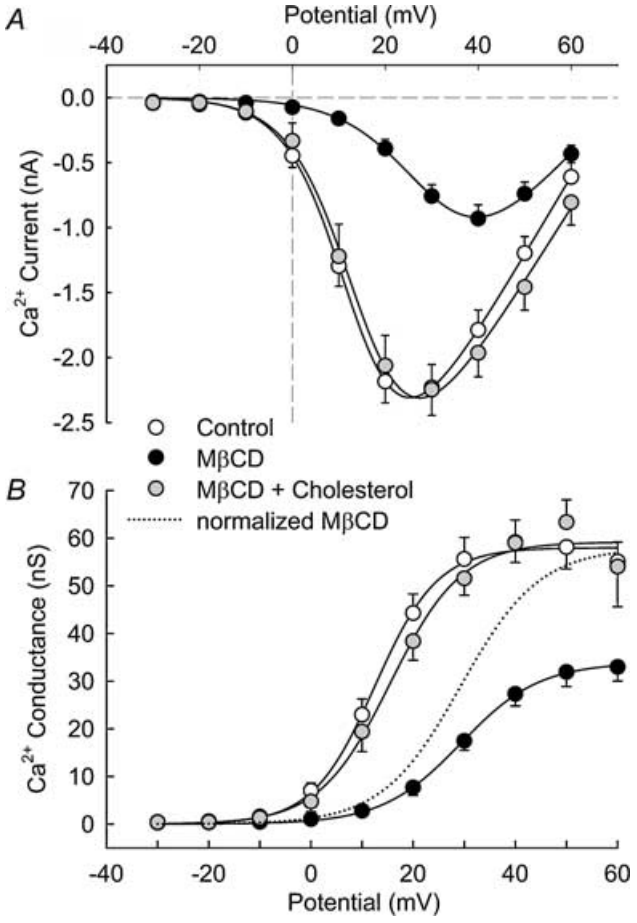

Figure 5. Cholesterol-saturated MβCD does not significantly affect L-type Ca^{2+} current

A, voltage dependence of the average L-type Ca^{2+} current recorded in 32 control, 20 MβCD-treated and 9 cholesterol + MβCD-treated fibres. Continuous lines correspond to a fit to the mean data using eqn (1) from Methods. *B*, average voltage dependence of L-type macroscopic conductance in control ($n = 32$), MβCD-treated ($n = 20$) and cholesterol + MβCD-treated ($n = 9$) fibres. Continuous lines correspond to a Boltzmann fit to the average populations. The parameters of the fit are $G_{max} = 58.0$, 33.9 and 57.2 nS, $V_{1/2,G} =$ 12.5, 29.3 and 15.5 mV, $k_G = 6.11$, 7.70 and 6.94 mV for control, MβCD-treated and cholesterol + MβCD-treated cells, respectively. The dotted line corresponds to the normalization of the fit obtained in MβCD-treated cells with respect to the G_{max} value determined under control conditions.

Since the L-type Ca^{2+} current is sensitive to DHPs, we evaluated possible changes in sensitivity to the DHP agonist Bay K 8644. Figure 7 shows the effect of external application of 5 μM Bay K 8644 to control and MβCD-treated myofibres. In these experiments, data were fitted with eqn (1) as described in Methods to determine I_{max}, which corresponds to the peak of the *I–V* curve. For each cell, the maximum current during a step depolarization, recorded before and after Bay K 8644 application, was normalized with respect to the value of I_{max} obtained during the control period. The graphs shown were obtained by averaging data from six control (Fig. 7*A*) and five MβCD-treated (Fig. 7*B*) myotubes. In agreement with previous results (Strube *et al.* 1996), Bay K 8644 treatment in control cells increased I_{max} by ∼1.4-fold and shifted its peak towards negative potentials by ∼8.5 mV. In MβCD-treated cells, the increase was significantly larger (∼1.96-fold) and the potential of half-activation, $V_{1/2,G}$, was slightly more shifted, suggesting a change in the DHP sensitivity. These results show that a saturating concentration of Bay K 8644 facilitated activation more in MβCD-treated than in control cells.

The impact of MβCD treatment on DHP receptor function in myofibres E–C coupling was inferred from intramembrane charge movements and from Ca^{2+} transients evoked by voltage. Figure 8*A* shows

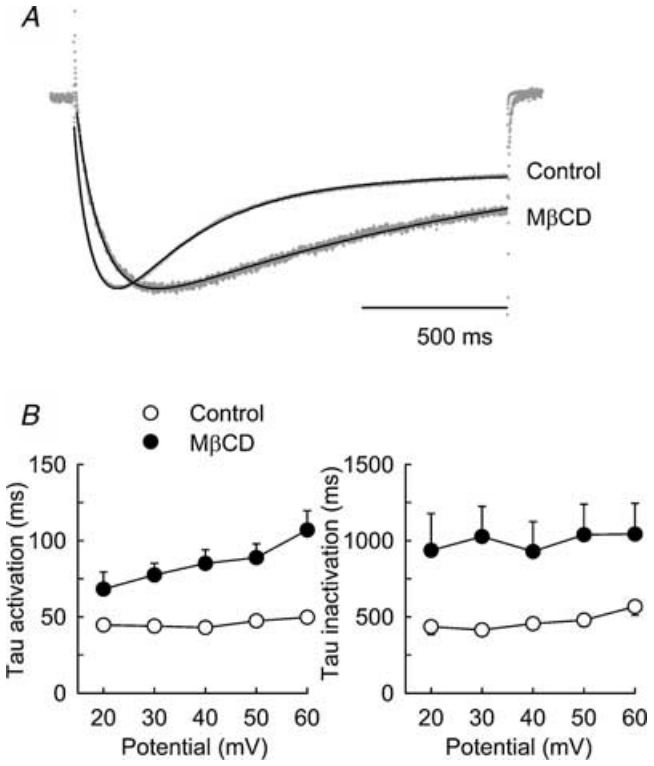

Figure 6. MβCD treatment slows down L-type Ca^{2+} current activation and inactivation kinetics
A, traces of Ca^{2+} current normalized with respect to the peak recorded in control and MβCD-treated myofibres in response to a 1500 ms depolarizing pulse to +30 mV. The continuous thin lines correspond to a fit of the current recordings using eqn (1) from Methods. *B*, voltage dependence of the activation (left) and inactivation (right) time constants of L-type Ca^{2+} current obtained by fitting the current recordings shown in *A*. Values are mean ± S.E.M. obtained in 24 control and 16 MβCD-treated myofibres.

representative asymmetrical currents produced by charge movements in response to 2 of 12 depolarizing pulses delivered to each cell (−10 and +60 mV). Traces show a transient current at the onset of the voltage step, the ON charge, and an equal inverted current at the end of the voltage step, the OFF charge. The voltage dependence of the ON charge estimated by integration is shown in Fig. 8*B*. In all cases, charge movement did not occur at potentials more negative than −30 mV, then increased in a sigmoidal fashion and saturated at potentials more positive than +30 mV. These data were adequately fitted by Boltzmann equations shown by the lines. Boltzmann parameters determined for each cell and then averaged are given for control and MβCD-treated cells in Table 3. Figure 8*B* and Table 3 show that the magnitude of charge movements evoked in MβCD-treated myotubes was smaller than in control conditions at all potentials. The maximum amount of charge evoked was reduced ∼30% after MβCD treatment. However, MβCD treatment did not affect the voltage dependence of charge movement as shown by the normalization of the data obtained in MβCD-treated fibres (dotted line of Fig. 8*B*). The alteration of intramembrane charge movement by MβCD should also be reflected in voltage-evoked Ca^{2+} transient properties. Changes in intracellular Ca^{2+} concentration in response to depolarization were evaluated using confocal line-scan imaging of fluo-4 fluorescence as described in Methods. Figure 9*A* shows the time course of the fluo-4 fluorescence intensity in control and MβCD-treated cells in response to a 50 ms depolarization to the indicated potential from a holding potential of −80 mV. In both

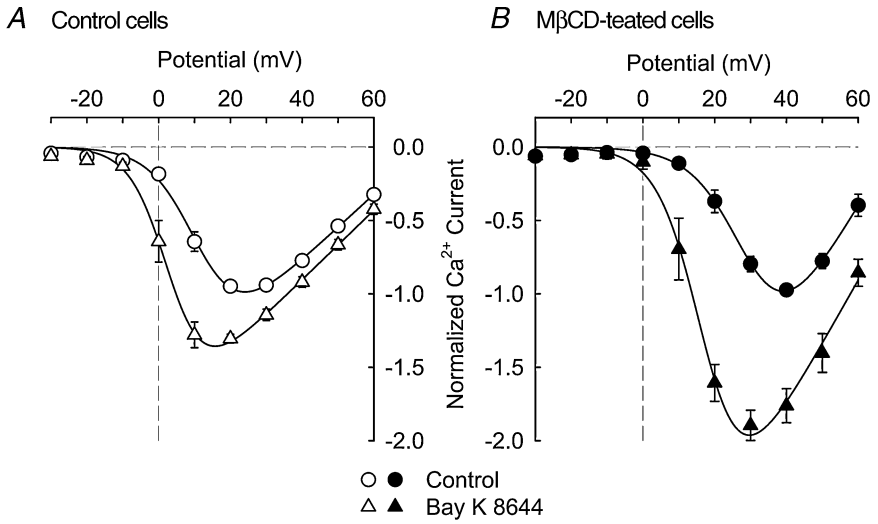

Figure 7. MβCD treatment enhances stimulation of L-type Ca^{2+} current by Bay K 8644
A, average *I–V* curves compiled from recordings from 6 control cells before and after application of 5 μM Bay K 8644. L-type current amplitudes have been normalized to the maximum current amplitude measured before Bay K 8644 application. *B*, same curves as in *A* but obtained from 5 MβCD-treated cells.

cases, the increase in cytosolic Ca^{2+} started at the onset of the depolarization, peaked less than 100 ms later and had a relatively long recovery time (>1 s). However, the peak of the fluorescence was smaller in MβCD-treated cells. The voltage dependence of $\Delta F/F_0$ measured at the peak of the transient is shown in Fig. 9*B*. In control and MβCD-treated myotubes, the peak transient had a threshold at ~-10 mV, increased with pulse potential from -10 to $+50$ mV and reached a plateau at more positive potentials. Table 3 and Fig. 9*B* show that the maximum peak fluorescence change (F_{max}) was reduced by $\sim$45% after MβCD treatment. However, as for charge movements, MβCD treatment did not affect the voltage dependence of Ca^{2+} transients as shown by the normalization of the data obtained in MβCD-treated fibres (dotted line of Fig. 9*B*). Altogether these results show that MβCD treatment weakened E–C coupling without affecting its voltage dependence.

Discussion

The cholesterol-binding drug MβCD has been widely used to reduce the cholesterol content of the plasma membrane in single cell assays (Kilsdonk *et al.* 1995; Yancey *et al.* 1996; Christian *et al.* 1997; Gimpl *et al.* 1997; Steck *et al.* 2002). Our data show that exposure of freshly isolated skeletal muscle cells to MβCD led to striking morphological modifications accompanied by changes in DHPR function. MβCD has been suggested to remove membrane

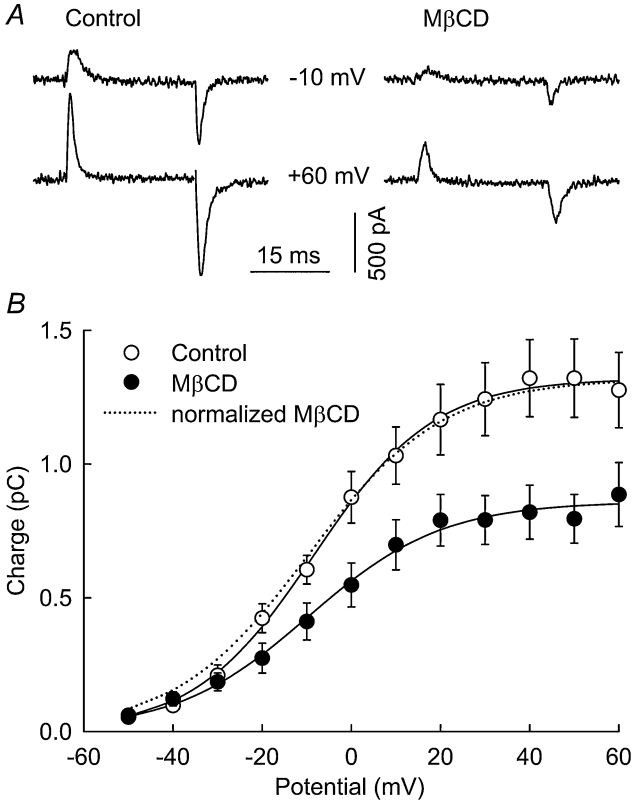

Figure 8. MβCD treatment decreases intramembrane charge movement without significantly affecting voltage dependence
A, charge movement recordings obtained in response to 25 ms pulses from a holding potential of -80 mV to the indicated potential in control and MβCD-treated fibres. *B*, average voltage dependence of charge moved in response to depolarization estimated by integration of the current recorded in 14 control and 17 MβCD-treated cells. Continuous lines correspond to a Boltzmann fit to the average populations. Parameters of the fit are $Q_{max} = 1.32$ and 0.86 pC, $V_{1/2,Q} = -8.4$ and -9.7 mV and $k_Q = 13.5$ and 15.0 mV for control and MβCD-treated cells, respectively. The dotted line corresponds to the normalization of the fit obtained in MβCD-treated cells with respect to the Q_{max} value determined under control conditions.

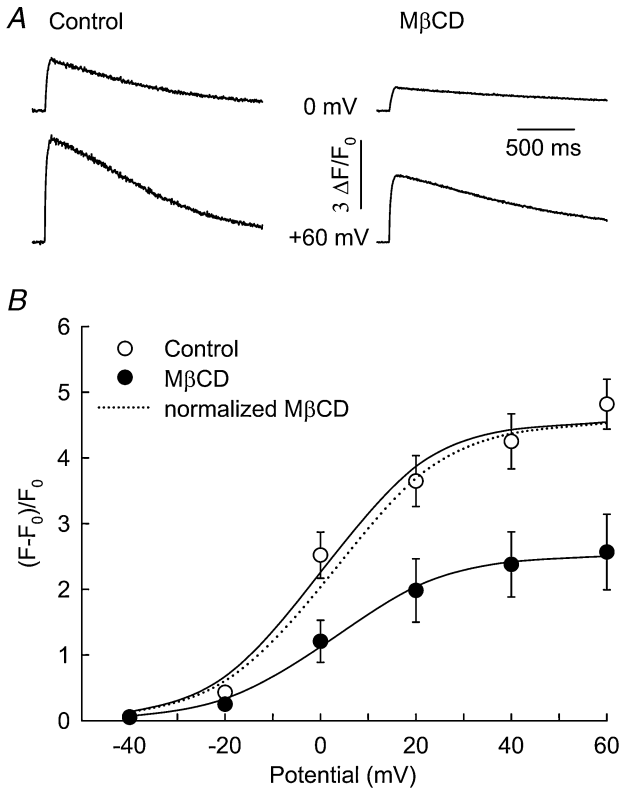

Figure 9. MβCD treatment decreases Ca^{2+} transients without significantly affecting their voltage dependence
A, time course of the fluo-4 fluorescence intensity in response to 50 ms pulses from a holding potential of -80 mV to the indicated potential recorded in control and MβCD-treated fibres. *B*, average voltage dependence of the fluorescence variation recorded from 10 control and 9 MβCD-treated cells. Continuous lines correspond to a Boltzmann fit to the average populations. Parameters of the fit are $F_{max} = 4.6$ and 2.5, $V_{1/2,F} = 0.2$ and 2.7 mV and $k_F = 11.5$ and 12.1 mV for control and MβCD-treated cells, respectively. The dotted line corresponds to the normalization of the fit obtained in MβCD-treated cells with respect to the F_{max} value determined under control conditions.

Table 3. Parameter values of *Q–V* and *F–V* curve fits

	Q – *V* data				*F* – *V* data			
	n	Q_{max} (pC)	$V_{1/2,Q}$ (mV)	k_Q (mV)	*n*	F_{max}	$V_{1/2,F}$ (mV)	k_F (mV)
Control	14	1.30 ± 0.13	−7.9 ± 2.4	13.4 ± 1.0	10	4.7 ± 0.3	3.0 ± 3.2	11.8 ± 1.3
MβCD	17	0.95 ± 0.11*	−4.6 ± 3.1	14.5 ± 0.9	9	2.8 ± 0.5*	9.5 ± 2.8	14.4 ± 1.3

All the parameters were calculated as described in Methods. Q_{max} and F_{max} are the maximum amount of evoked charge movement and the maximum variation of fluorescence, respectively; $V_{1/2,Q}$ and $V_{1/2,F}$ are the potentials that elicit the half-maximum increases for *Q* or *F*, respectivley, and *k* is a slope factor. Data are given as mean ± S.E.M and were obtained by fitting the data from *n* fibres in each group. *Values which are significantly different from the corresponding control values ($P < 0.04$, Mann-Whitney test).

cholesterol by a mechanism involving cholesterol diffusion directly from the plasma membrane into the hydrophobic core of the MβCD molecule packed near the membrane surface, without the necessity of desorbing completely into the aqueous phase (Yancey *et al.* 1996). In the present experiments, the lack of effect of MβCD treatment on the T-type Ca^{2+} current provided a critical internal control and suggested that, amongst muscle voltage-dependent Ca^{2+} channels, MβCD specifically targets DHPRs. Moreover, action potentials recorded in control and MβCD-treated cells appeared similar suggesting that action potential propagation along the surface membrane as well as along T-tubules was not drastically affected by the treatment. These controls suggest that the observed effects of MβCD treatment on DHPR were not consequences of a general effect of cholesterol removal on general membrane physiology that could lead to drastic alterations of all ions channels. The hypothesis of a direct pharmacological effect of MβCD on DHPRs was ruled out by preloading MβCD with cholesterol prior to exposure to the fetal cells. Cholesterol-saturated MβCD did not reproduce the effect of MβCD alone. Neither the amplitude nor voltage dependence of the L-type Ca^{2+} current were affected, and cholesterol-saturated MβCD even induced a decrease in the time to peak of L-type Ca^{2+} current (most likely due to membrane cholesterol enrichment; results not shown) whereas MβCD alone increased this parameter. Thus, in accordance with results obtained by Launikonis & Stephenson (2001) on skinned toad muscle fibres, our results show that MβCD *per se* does not have a pharmacological effect on DHPRs, but acts via retrieval of cholesterol from the membrane.

Membrane cholesterol depletion of skeletal muscle cells caused a significant decrease in morphologically recognizable caveolae, together with an ∼30% reduction in the extent of surface-connected tubular elements. These morphometric results, obtained with freshly dissociated differentiated muscle fibres, confirm the previous determinations obtained on C2C12 muscle cell cultures using the cholesterol-binding drug Amphotericin B (Carozzi *et al.* 2000). In voltage-clamp experiments, MβCD treatment reduced the membrane electrical capacitance by ∼25%. This decrease in electrical capacitance cannot be explained by changes in the electrical properties of the membrane since straightforward considerations predict an increase in membrane capacitance upon cholesterol removal. If we assume that the membrane is analogous to a parallel-plate capacitor with an insulator of dielectric constant ε and thickness *d,* then the specific membrane capacitance, i.e. the capacitance value of a 1 cm^2 area of membrane, namely *C*, is (Hille, 1992):

$$C = \varepsilon \times \varepsilon_0 / d$$

where ε_0 is the polarizability of free space. Because the membrane dielectric constant in the presence of cholesterol is not significantly different from that in the presence of other lipids (Fettiplace *et al.* 1975) and considering that the inclusion of cholesterol in a membrane tends to increase the geometric thickness of the bilayer (Yeagle, 1985; Tulenko *et al.* 1998), the equation above predicts that *C* should increase when cholesterol is removed from the plasma membrane. The fact that we observe the opposite effect, i.e. a decrease in membrane capacitance with cholesterol depletion, suggests that MβCD induced a significant loss of plasma membrane and/or plasma membrane-connected tubular membranes and thus confirms our morphometric data.

Table 4 summarizes the effect of MβCD on several experimental parameters investigated in the present study. This table indicates that MβCD did not significantly affect the visual surface or the T-type Ca^{2+} current amplitude. Other parameters were reduced, although not all in the same proportion. For instance, we observed a 25% reduction in electrical capacitance, whereas the L-type Ca^{2+} conductance was reduced by 41%. Besides, the total amount of intramembrane charge movements was reduced by 27%. Part of the observed decrease in L-type Ca^{2+} conductance and charge movement could

Table 4. Effect of MβCD on several parameters

	Control	n_1	MβCD	n_2	Decrease
Surface (μm^2)	10773 ± 510	21	10106 ± 533	36	Not significant
Capacitance (pF)	278 ± 14	52	209 ± 12	57	25%
I_T (nA)	-549 ± 63	38	-615 ± 56	40	Not significant
I_L (nA)	-2.58 ± 0.18	38	0.85 ± 0.09	40	67%
G_{max} (nS)	58.8 ± 4.5	32	34.5 ± 2.9	20	41%
G_{max} (pS pF^{-1})	204 ± 13	32	169 ± 17	20	17%
Q_{max} (fC)	1.30 ± 0.13	14	0.95 ± 0.11	17	27%
Q_{max} (fC pF^{-1})	5.58 ± 0.42	14	4.74 ± 0.49	17	15%
F_{max}	4.7 ± 0.3	10	2.8 ± 0.5	9	40%

All the parameters were calculated as described in Methods. I_T is the amplitude of T-type Ca^{2+} current at -20 mV, I_L is the peak of the I_L–V curve, G_{max} is the maximum conductance for L-type Ca^{2+} current, Q_{max} is the maximum amount of evoked charge movement and F_{max} is the maximum variation of fluorescence in response to a depolarization. Averages of G_{max} in pS pF^{-1} and Q_{max} in fC pF^{-1} have been calculated by dividing the value of G_{max} or Q_{max} of each studied cell by it's own capacitance. The percentage reduction is indicated when the values obtained for control and MβCD-treated cells were significantly different ($P < 0.05$, Mann–Whitney test).

result from the loss of electrical connectivity between a fraction of DHPR-containing membrane domains, comprising caveolae and developing T-tubules, and the cell surface membrane, as suggested by the observed decrease in capacitance and our morphometric results. These results are in accordance with previous studies describing a significant decrease in Ca^{2+} current after detubulation by glycerol treatment (Siri *et al.* 1980; Potreau & Raymond, 1980; Almers *et al.* 1981; Romey *et al.* 1989). However, normalization of the conductance and the amount of charge movement by the capacitance still reveals a 17% reduction in G_{max} and 15% reduction in Q_{max}, indicating that the macroscopic conductance and charge movements were significantly more affected by MβCD treatment than the capacitance. Moreover, gating properties of L-type channels, such as the half-activation potential, the activation and inactivation kinetics and the modulation by Bay K 8466 were affected by membrane cholesterol depletion. It is important to note here that we obtained qualitatively similar results (reduction of L-type current amplitude, positive shift of the voltage dependence and slowing down of the time to peak) with myofibres from 15-day-old fetuses where the T-tubule system is absent (Franzini-Armstrong, 1991), indicating that the observed effects could not be attributed to a space clamp bias. Thus, cholesterol removal appeared to have a stronger effect on DHPR expression than predicted on the basis of the loss in electrical capacitance. The supplementary reduction of G_{max} and Q_{max} could be explained by a heterogeneous distribution of the DHPRs in the cell membrane (i.e. a higher concentration in the invaginations which are disconnected from the surface sarcolemma by MβCD treatment). In addition, the functional expression of the DHPRs present in the membrane domains still electrically connected to the cell surface is likely to have been altered by the reduced amount of cholesterol in the membrane. Indeed, membrane cholesterol content has been shown to influence not only membrane fluidity but also dipole potential which plays an important role in modulating membrane function (Szabo, 1974; Brockman, 1994), and could in particular affect the conductance and gating properties of ion channels (Moczydlowski *et al.* 1985; Jordan, 1987; Bolotina *et al.* 1989; Chang *et al.* 1995). Alternatively, the observed effects on L-type Ca^{2+} current upon cholesterol removal could reflect changes in the interaction of DHPRs with surrounding proteins located in caveolae and T-tubules, such as caveolin-3. Indeed, cholesterol has been shown to play a critical role in maintaining the caveolae membrane domains (Rothberg *et al.* 1992). Furthermore, caveolin-3 is a cholesterol-interacting protein highly concentrated in caveolae and T-tubules and has been shown to functionally interact with different ion channels (for review see Razani *et al.* 2002). The hypothesis of a functional link between L-type Ca^{2+} channels and caveolin has thus to be considered, although the existence and the nature of the molecular interactions involved need to be further explored.

The fluorescence measurements showed a reduction of voltage-gated Ca^{2+} transients, indicating a weakening of E–C coupling in MβCD-treated fibres. This could be explained by the combination of the decrease in charge movement, a modification of the functional properties of the sarcoplasmic reticulum and a more general effect of cholesterol depletion on muscle physiology. Indeed, due to intracellular cholesterol trafficking, surface membrane

cholesterol removal could induce the subsequent depletion in cholesterol of the sarcoplasmic reticulum membrane, that could in turn alter the Ca^{2+} handling abilities of the sarcoplasmic reticulum, as shown by Launikonis & Stephenson (2001). Cheng *et al.* (1986) also showed that cholesterol content could affect Ca^{2+}-ATPase activity. Thus, it would be interesting in the future to test if the Ca^{2+} release flux and the gating of the ryanodine receptor can be altered by MβCD treatment. Further, it is important to note that MβCD treatment did not affect the voltage dependence of E–C coupling whereas that of the L-type current in MβCD-treated cells was shifted by more than 15 mV towards positive potentials compared to control cells. Overall, the change in membrane cholesterol content appears to differentially modulate the two functional expressions of the DHPR as a voltage sensor for E–C coupling and as an L-type Ca^{2+} channel. These results strengthen the previously proposed hypothesis of the possible existence of two different subpopulations of DHPRs (Strube *et al.* 1992, 2000).

In the above-mentioned previous work, a differential regulation of the two functions of the DHPR was observed during prenatal myogenesis; intriguingly, some of the properties observed after MβCD treatment are reminiscent of those of skeletal muscle cells seen at earlier stages of development. The transverse tubular system of MβCD-treated cells had a pronounced longitudinal orientation, comparable to that seen during early gestation (Franzini-Armstrong, 1991; Takekura *et al.* 2001). L-type Ca^{2+} currents recorded in early prenatal (E14) mice skeletal muscle cells are characterized by a positive shift of the voltage dependence and a slower time to peak compared to currents recorded around birth (E18–E19) (Strube *et al.* 2000). Moreover, the L-type current has a higher sensitivity to Bay K 8644 in E14 myofibres than in E18 myofibres (authors' unpublished data). Compared to these results, membrane cholesterol depletion seems to modify L-type Ca^{2+} current properties by mimicking effects observed at earlier stages of development. However, MβCD treatment may not accurately reproduce the physiological changes in membrane cholesterol content and this could account for the slight differences observed regarding parameters such as the activation kinetics, which do not change during development whereas they are slowed down by MβCD treatment. Moreover, it is worth emphasizing that studies evaluating membrane cholesterol during development are in disagreement. In *in vivo* studies, a decrease in membrane cholesterol content was observed during development in chicken and rabbit skeletal muscle (Boland & Martonosi, 1974; Smith & Clark, 1980; Volpe *et al.* 1982), whereas an increase in membrane cholesterol content was reported during development in cultured chicken muscle cells (Boland *et al.* 1977). Thus, it would be interesting to determine the variations of membrane cholesterol in our system to evaluate a possible role of cholesterol in DHPR modulation during myogenesis.

In conclusion, our results show that cholesterol plays an important role in fetal skeletal muscle cells and can modulate the functional expression of DHPRs. Membrane cholesterol depletion by MβCD leads to (1) a disruption of T-tubules and caveolae containing DHPRs and thus a decrease in the number of functional DHPRs; (2) a modulation of the functional expression of the remaining DHPRs, including important modifications of the L-type Ca^{2+} channel gating properties. The decrease in intramembrane charge movements and Ca^{2+} transients indicates an impairment of E–C coupling function and confirms, in freshly isolated mammalian cells, the results obtained by Launikonis & Stephenson (2001) using toad skinned fibres, in which depletion of membrane cholesterol caused a weakening of E–C coupling. Regarding L-type Ca^{2+} channel function, the alteration of gating properties (15 mV positive shift of the *I–V* curve and slowing down of the activation and inactivation kinetics) indicates a direct effect of membrane cholesterol content on the DHPR and suggests a modulation of the open probability and/or the single channel current by cholesterol, over and above the decrease in the number of functional channels. Previous studies on muscle are, to our knowledge, restricted to smooth and cardiac muscles and the literature reveals discrepancies. In smooth muscle, Gleason *et al.* (1991) and Sen *et al.* (1992) reported an increase in L-type Ca^{2+} current with membrane cholesterol enrichment using arterial muscle cell cultures. Additionally, Renaud *et al.* (1986) and Bergdahl *et al.* (2003) reported, in cardiac and smooth muscle cells, respectively, an inhibition of L-type calcium current by a statin called lovastatin, which was also shown to reduce plasma membrane cholesterol in brain cells (Kirsch *et al.* 2003). However, Jennings *et al.* (1999) observed an inhibition of Ca^{2+} current by cholesterol in gallbladder smooth muscle and Löhn *et al.* (2000) showed that cholesterol depletion did not affect L-type current in arterial and cardiac muscle cells. In our case, cholesterol depletion induced a decrease in L-type Ca^{2+} current. Such diverse effects of cholesterol on DHPR function could reflect differences in cholesterol-enriched microdomains, or variations in density of transverse tubules and types of DHPR in the different muscle cell types investigated. Taking this into account, it appears fundamental to pursue studies in mammalian

skeletal muscle fibres *in vivo* to further understand how membrane cholesterol content can regulate the L-type Ca^{2+} channel function and the voltage-sensor function of the DHPR in both developing and adult mammalian skeletal muscle. Such studies are of particular interest for skeletal muscle physiopathology mechanisms as mild-to-severe myopathies have been reported to be possible adverse effects of blood-cholesterol-lowering treatments using statins (Thompson *et al.* 2003), which, as mentioned above, can alter L-type Ca^{2+} current as well as membrane cholesterol content (Renaud *et al.* 1986; Bergdahl *et al.* 2003; Kirsch *et al.* 2003).

References

Adams BA, Tanabe T, Mikami A, Numa S & Beam KG (1990). Intramembrane charge movement restored in dysgenic skeletal muscle by injection of dihydropyridine receptor cDNAs. *Nature* **346**, 569–572.

Ahern CA, Powers PA, Biddlecome GH, Roethe L, Vallejo P, Mortenson L, Strube C, Campbell KP, Coronado R & Gregg RG (2001). Modulation of L-type Ca2+ current but not activation of Ca2+ release by the gamma1 subunit of the dihydropyridine receptor of skeletal muscle. *BMC Physiol* **1**, 8.

Almers W, Fink R & Palade PT (1981). Calcium depletion in frog muscle tubules: the decline of calcium current under maintained depolarisation. *J Physiol* **312**, 177–207.

Bastiaanse EM, Atsma DE, Kuijpers MM & Van der Laarse A (1994). The effect of sarcolemmal cholesterol content on intracellular calcium ion concentration in cultured cardiomyocytes. *Arch Biochem Biophys* **313**, 58–63.

Bastiaanse EM, Hold KM & Van der Laarse A (1997). The effect of membrane cholesterol content on ion transport processes in plasma membranes. *Cardiovasc Res* **33**, 272–283.

Beam KG & Knudson CM (1988). Effect of postnatal development on calcium currents and slow charge movement in mammalian skeletal muscle. *J General Physiol* **91**, 799–815.

Bergdahl A, Persson E, Hellstrand P & Swärd K (2003). Lovastatin induces relaxation and inhibits L-type Ca2+ current in the rat basilar artery. *Pharmacol Toxicol* **93**, 128–134.

Berthier C, Monteil A, Lory P & Strube C (2002). Alpha(1H) mRNA in single skeletal muscle fibres accounts for T-type calcium current transient expression during foetal development in mice. *J Physiol* **539**, 681–691.

Biederer CH, Ries SJ, Moser M, Florio M, Israel MA, McCormick F & Buettner R (2000). The basic helix-loop-helix transcription factors myogenin and Id2 mediates specific induction of caveolin-3 gene expression during embryonic development. *J Biol Chem* **34**, 26245–26251.

Bijlenga P, Liu J-H, Espinos E, Haenggli C-A, Fischer-Lougheed J, Bader CR & Bernheim L (2000). T-type alpha1H Ca2+ channels are involved in Ca2+ signaling during terminal differentiation (fusion) of human myoblasts. *Proc Natl Acad Sci U S A* **97**, 7627–7632.

Boland R, Chyn T, Roufa D, Reyes E & Martonosi A (1977). The lipid composition of muscle cells during development. *Biochim Biophys Acta* **489**, 349–359.

Boland R & Martonosi A (1974). Developmental changes in the composition and function of sarcoplasmic reticulum. *J Biol Chem* **249**, 612–623.

Bolotina V, Omelyanenko V, Heyes B, Ryan U & Bregestovski P (1989). Variations of membrane cholesterol alter the kinetics of Ca2+-dependent K+ channels and membrane fluidity in vascular smooth muscle cells. *Pflugers Arch* **415**, 262–268.

Brockman H (1994). Dipole potential of lipid membranes. *Chem Physics Lipids* **73**, 57–79.

Carozzi AJ, Ikonen E, Lindsay MR & Parton RG (2000). Role of cholesterol in developing T-tubules: analogous mechanisms for T-tubule and caveolae biogenesis. *Traffic* **1**, 326–341.

Chang HM, Reitstetter R, Mason RP & Gruener R (1995). Attenuation of channel kinetics and conductance by cholesterol: an interpretation using structural stress as a unifying concept. *J Membr Biol* **143**, 51–63.

Chang WJ, Rothberg KG, Kamen BA & Anderson RG (1992). Lowering cholesterol content of MA104 cells inhibits receptor-mediated transport of folate. *J Cell Biol* **118**, 63–69.

Cheng KH, Lepock JR, Hui SW & Yeagle PL (1986). The role of cholesterol in the activity of reconstituted Ca-ATPase vesicles containing unsaturated phosphatidylethanolamine. *J Biol Chem* **261**, 5081–5087.

Christian AE, Haynes MP, Phillips MC & Rothblat GH (1997). Use of cyclodextrins for manipulating celllular cholesterol content. *J Lipid Res* **38**, 2264–2272.

Fettiplace R, Gordon LGM, Hladky SB, Requena J, Zingsheim HP & Haydon DA (1975). Techniques in the formation and examination of 'black' lipid bilayer membranes. In Methods in Membrane Biology, vol. 4, ed. Korn ED, pp. 1–75. Plenum Press, New York and London.

Flucher BE, Terasaki M, Chin HM, Beeler TJ & Daniels MP (1991). Biogenesis of transverse tubules in skeletal muscle in vitro. *Dev Biol* **145**, 77–90.

Franzini-Armstrong C (1991). Simultaneous maturation of transverse tubules and sarcoplasmic reticulum during muscle differentiation in the mouse. *Dev Biol* **146**, 353–363.

Gimpl G, Burger K & Fahrenholz F (1997). Cholesterol as modulator of receptor function. *Biochemistry* **36**, 10959–10974.

Gleason MM, Medow MS & Tulenko TN (1991). Excess membrane cholesterol alters calcium movements, cytosolic calcium levels, and membrane fluidity in arterial smooth muscle cells. *Circ Res* **69**, 216–227.

Hailstones D, Sleer LS, Parton RG & Stanley KK (1998). Regulation of caveolin and caveolae by cholesterol in MDCK cells. *J Lipid Res* **39**, 369–379.

Hille B (1992). Ionic Channels in Excitable Membrane, 2nd edn. Sinauer Associates Inc, Sunderland, MA, USA.

Ishikawa H (1968). Formation of elaborate networks of T-system tubules in cultured skeletal muscle with special reference to the T-system formation. *J Cell Biol* **38**, 51–66.

Isshiki M & Anderson RGW (1999). Calcium signal transduction from caveolae. *Cell Calcium* **26**, 201–208.

Jennings LJ, Xu Q-W, Nelson MT & Mawe GM (1999). Cholesterol inhibits spontaneous action potentials and calcium currents in guinea pig gallbladder smooth muscle. *Am J Physiol* **277**, G1017–G1026.

Jordan PC (1987). How pore mouth charge distributions alter the permeability of transmembrane ionic channels. *Biophys J* **51**, 297–311.

Jorgensen AO, Shen AC-Y, Arnold W, Leung AT & Campbell KP (1989). Subcellular distribution of the 1,4-dihydropyridine receptor in rabbit skeletal muscle in situ: an immunofluorescence and immunocolloidal gold-labeling study. *J Cell Biol* **109**, 135–147.

Kilsdonk EP, Yancey PG, Stoudt GW, Bangerter FW, Johnson WJ, Phillips MC & Rothblat GH (1995). Cellular cholesterol efflux mediated by cyclodextrins. *J Biol Chem* **270**, 17250–17256.

Kirsch C, Eckert GP & Mueller WE (2003). Statin effects on cholesterol micro-domains in brain plasma membranes. *Biochem Pharmacol* **65**, 843–856.

Launikonis BS & Stephenson DG (2001). Effects of membrane cholesterol manipulation on excitation-contraction coupling in skeletal muscle of the toad. *J Physiol* **534**, 71–85.

Löhn M, Furstenau M, Sagach V, Elger M, Schulze W, Luft FC, Haller H & Gollasch M (2000). Ignition of calcium sparks in arterial and cardiac muscle through caveolae. *Circ Res* **87**, 1034–1039.

Minetti C, Bado M, Broda P, Sotgia F, Bruno C, Galbiati F, Volonte D, Lucania G, Pavan A, Bonilla E, Lisanti M & Cordone G (2002). Impairment of caveolae formation and T-system disorganization in human muscular dystrophy with caveolin-3 deficiency. *Am J Pathol* **160**, 265–270.

Moczydlowski E, Alvarez O, Vergara C & Latorre R (1985). Effect of phospholipid surface charge on the conductance and gating of a Ca2+-activated K+ channel in planar lipid bilayers. *J Membr Biol* **83**, 273–282.

Morris GE & Cole RJ (1979). Calcium and the control of muscle-specific creatine kinase accumulation during skeletal muscle differentiation in vitro. *Dev Biol* **69**, 146–158.

Parton RG, Way M, Zorzi N & Stang E (1997). Caveolin-3 associates with developing T-tubules during muscle differentiation. *J Cell Biol* **136**, 137–154.

Potreau D & Raymond G (1980). Slow inward barium current and contraction on frog single muscle fibres. *J Physiol* **303**, 91–109.

Pouvreau S, Berthier C, Blaineau S, Amsellem J, Coronado R & Strube C (2003). Cholesterol modulates dihydropyridine receptor function in foetal skeletal muscle cells. *Biophys J* **84**, 329A.

Ralston E & Ploug T (1999). Caveolin-3 associated with the T-tubules of mature skeletal muscle fibres. *Exp Cell Res* **246**, 510–515.

Razani B, Woodman SE & Lisanti MP (2002). Caveolae: from cell biology to animal physiology. *Pharmacol Rev* **54**, 431–467.

Renaud JF, Schmid A, Romey G, Nano JL & Lazdunski M (1986). Mevinolin, an inhibitor of cholesterol biosynthesis, drastically depresses Ca2+ channel activity and uncouples excitation from contraction in cardiac cells in culture. *Proc Natl Acad Sci U S A* **83**, 8007–8011.

Rios E & Brum G (1987). Involvement of dihydropyridine receptor in excitation-contraction coupling in skeletal muscle. *Nature* **325**, 717–720.

Romey G, Garcia L, Dimitriadou V, Pincon-Raymond M, Rieger F & Lazdunski M (1989). Ontogenesis and localization of Ca2+ channels in mammalian skeletal muscle in culture and role in excitation-contraction coupling. *Proc Natl Acad Sci U S A* **86**, 2933–2937.

Rosemblatt M, Hidalgo C, Vergara C & Ikemoto N (1981). Immunological and biochemical properties of transverse tubule membranes isolated from rabbit skeletal muscle. *J Biol Chem* **256**, 8140–8148.

Rothberg KG, Heuser JE, Donzell WC, Ying YS, Glenney JR & Anderson RG (1992). Caveolin, a protein component of caveolae membrane coats. *Cell* **21**, 673–682.

Rothberg KG, Ying YS, Kamen BA & Anderson RG (1990). Cholesterol controls the clustering of the glycophospholipid-anchored membrane receptor for 5-methyltetrahydrofolate. *J Cell Biol* **111**, 2931–2938.

Salzberg S, Mandelboim M, Zalcberg M, Shainberg A & Mandelbaum M (1995). Interruption of myogenesis by transforming growth factor beta1 or EGTA inhibits expression and activity of the myogenic-associated (2′-5′) oligoadenylate synthetase and PKR. *Exp Cell Res* **219**, 223–232.

Seigneurin-Venin S, Parrish E, Marty I, Rieger F, Romey G, Villaz M & Garcia L (1996). Involvement of the dihydropyridine receptor and internal Ca2+ stores in myoblast fusion. *Exp Cell Res* **223**, 301–307.

Sen L, Bialecki RA, Smith E, Smith TW & Colucci WS (1992). Cholesterol increases the L-type voltage-sensitive calcium channel current in arterial smooth muscle cells. *Circ Res* **71**, 1008–1014.

Shacklock PS, Wier WG & Balke CW (1995). Local Ca2+ transients (Ca2+ sparks) originate at transverse tubules in heart cells. *J Physiol* **15**, 601–608.

Shainberg A, Yagil G & Yaffe D (1969). Control of myogenesis in vitro by Ca2+ concentration in nutritional medium. *Exp Cell Res* **58**, 163–167.

Shaul PW & Anderson RGW (1998). Role of plasmalemmal caveolae in signal transduction. *Am J Physiol* **275**, L843–L851.

Shimahara T & Bournaud R (1991). Barium current in developing skeletal muscle cells of normal and mutant mice foetuses with 'muscular dysgenesis'. *Cell Calcium* **12**, 727–733.

Siri NL, Sanchez JA & Stefani E (1980). Effect of glycerol treatment on the calcium current of frog skeletal muscle. *J Physiol* **305**, 87–96.

Smith PB & Clark GF (1980). β-Adrenergic receptor-adenylate cyclase alterations during the postnatal development of skeletal muscle. *Biochim Biophys Acta* **633**, 274–288.

Steck TL, Ye J & Lange Y (2002). Probing red cell membrane cholesterol movement with cyclodextrin. *Biophys J* **83**, 2118–2125.

Strube C, Beurg M, Powers PA, Gregg RG & Coronado R (1996). Reduced Ca2+ current, charge movement, and absence of Ca2+ transients in skeletal muscle deficient in dihydropyridine receptor beta 1 subunit. *Biophys J* **71**, 2531–2543.

Strube C, Bournaud R, Inoue I & Shimahara T (1992). Intramembrane charge movement in developing skeletal muscle cells from fetal mice. *Pflugers Arch* **421**, 572–577.

Strube C, Carbonneau L, Blaineau S, Coronado R & Berthier C (2002). Cholesterol depletion affects dihydropyridine receptor function in skeletal muscle cells. *Biophys J* **82**, 79A.

Strube C, Tourneur Y & Ojeda C (2000). Functional expression of the L-type calcium channel in mice skeletal muscle during prenatal myogenesis. *Biophys J* **78**, 1282–1292.

Szabo G (1974). Dual mechanism for the action of cholesterol on membrane permeability. *Nature* **252**, 47–49.

Takekura HL, Flucher BE & Franzini-Armstrong C (2001). Sequential docking, molecular differentiation, and positioning of T-tubule/SR junctions in developing mouse skeletal muscle. *Dev Biol* **239**, 204–214.

Takekura HL, Sun X & Franzini-Armstrong C (1994). Development of excitation-contraction coupling apparatus in skeletal muscle: peripheral and internal calcium release units are formed sequentially. *J Muscle Res Cell Motil* **15**, 102–118.

Thompson PD, Clarkson P & Karas RH (2003). Statin-associeted myopathy. *JAMA* **289**, 1681–1690.

Tulenko TN, Chen M, Mason PE & Mason RP (1998). Physical effects of cholesterol on arterial smooth muscle membranes: evidence of immiscible cholesterol domains and alterations in bilayer width during atherogenesis. *J Lipid Res* **39**, 947–956.

Volpe P, Damiani E, Salviati G & Margreth A (1982). Transitions in membrane composition during postnatal development of rabbit fast muscle. *J Muscle Res Cell Motil* **3**, 213–230.

Yancey PG, Rodrigueza WV, Kilsdonk EP, Stoudt GW, Johnson WJ, Phillips MC & Rothblat GH (1996). Cellular cholesterol efflux mediated by cyclodextrins. Demonstration of kinetic pools and mechanism of efflux. *J Biol Chem* **271**, 16026–16034.

Yeagle PL (1985). Cholesterol and cell membrane. *Biochim Biophys Acta* **822**, 267–287.

Yuan SH, Arnold W & Jorgensen AO (1990). Biogenesis of transverse tubules: immunocytochemical localization of a transverse tubular protein (TS28) and a sarcolemmal protein (SL50) in rabbit skeletal muscle developing in situ. *J Cell Biol* **110**, 1187–1198.

Yuan SH, Arnold W & Jorgensen AO (1991). Biogenesis of transverse tubules and triads: immunolocalization of the 1,4-dihydropyridine receptor, TS28, and the ryanodine receptor in rabbit skeletal muscle developing in situ. *J Cell Biol* **112**, 289–301.

Acknowledgements

We wish to thank Leon Espinosa and Yves Tourneur for judicious advice on image analysis and Leah Carbonneau who did preliminary Ca^{2+} transient experiments on cultured cells. We also thank Isabel Ann Lefevre for her help with proofreading. This study was supported by the Centre National de la Recherche Scientifique (CNRS), the Université Claude Bernard, the Association Française contre les Myopathies (AFM) and by National Institutes of Health Grants AR46448 and HL47053 to R.C. The ultrastructural part of the study was performed at the Centre Technologique des Microstructures, Université Claude Bernard, Villeurbanne, France. S.P. held a fellowship from the French ministry of Research and New Technologies.

Author's present address

C. Strube: LNPC, CNRS UMR 6150, Faculté Médecine Nord, Bd Pierre Dramard, 13916 Marseille Cedex 20, France.